

## Inelastic two-degree-of-freedom model for roof frame under airblast loading

Park, Jong Yil<sup>†</sup>

*Joint Modeling and Simulation Center, Agency for Defense Development, Yuseong P.O. Box 35,  
Daejeon 305-600, Korea*

Theodor Krauthammer

*Director of the Center for Infrastructure Protection and Physical Security,  
Goldsby Chair in Civil Engineering, Professor, Center for Infrastructure Protection and Physical Security  
(CIPPS), University of Florida, USA*

*(Received November 16, 2008, Accepted February 16, 2009)*

**Abstract.** When a roof frame is subjected to the airblast loading, the conventional way to analyze the damage of the frame or design the frame is to use single degree of freedom (SDOF) model. Although a roof frame consists of beams and girders, a typical SDOF analysis can be conducted only separately for each component. Thus, the rigid body motion of beams by deflections of supporting girders can not be easily considered. Neglecting the beam-girder interaction in the SDOF analysis may cause serious inaccuracies in the response values in both Pressure-Impulse curve (P-I) and Charge Weight-Standoff Diagrams (CWSD). In this paper, an inelastic two degrees of freedom (TDOF) model is developed, based on force equilibrium equations, to consider beam-girder interaction, and to assess if the modified SDOF analysis can be a reasonable design approach.

**Keywords:** SDOF; TDOF; P-I curve; roof frame; blast.

---

### 1. Introduction

Design of buildings to resist airblast loading is generally conducted by local component damage analysis and global building collapse analysis, based on the results of the component damage analysis. The prevalent method adopted by the US Department of Defense to analyze component damage for designing structures under airblast loading is the SDOF analysis (TM 5-1300 1990, TM 5-855-1 1986). A SDOF analysis represents an equivalent one-degree system having a stiffness and mass for practical design purposes, which simplifies the analysis of structures with continuous mass distribution. For example, following is a SDOF-based governing equation of a beam without damping:

---

<sup>†</sup> Senior Researcher, Corresponding author, E-mail: [jongyilpark@gmail.com](mailto:jongyilpark@gmail.com)

$$K_{M\_b}M_b\ddot{u}_b(t) + K_{L\_b}R_b(u_b(t)) = K_{L\_b}F_b(t) \quad (1)$$

or

$$K_{LM\_b}M_b\ddot{u}_b(t) + R_b(u_b(t)) = F_b(t) \quad (2)$$

where

- $u_b(t)$  : beam midspan deflection;
- $M_b$  : total mass of beam;
- $R_b(u_b(t))$  : resistance of beam;
- $F_b(t)$  : applied force;
- $K_{M\_b}$  : mass factor of beam;
- $K_{L\_b}$  : load factor of beam, and
- $K_{LM\_b}$  : load-mass factor of beam =  $K_{M\_b}/K_{L\_b}$ .

where, the mass and load factors are determined to have the same energy distribution as that of the continuous beam responding in an assumed mode shape. Table 1 shows load, mass, and load-mass factors for beams with simply supported boundaries under uniformly distributed and concentrated loading conditions.

The following steps are performed when the SDOF model is the main analysis tool used to design a structural component under airblast loading (PDC-TR 06-08 2006):

- A. The maximum allowable ductility ratio and support rotation are determined by the level of protection for each building and the component types.
- B. A trial member is selected.
- C. The airblast load is estimated considering the charge weight, standoff distance, and the angle between the explosion point and the normal plane of the member.
- D. The maximum ductility ratio and support rotation of the member are calculated by using the SDOF method.
- E. The calculated maximum ductility ratio and support rotation are compared to the predetermined maximum allowable ductility ratio and support rotation.
- F. If the calculated response satisfies the allowable response, the design of the member is finalized. If not, the design is modified and the process is repeated.

Table 1 Load, Mass, and Load-Mass Factors (TM 5-855-1 1986)

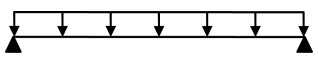
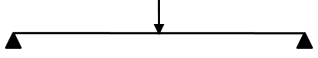
Edge Conditions and Loading Diagrams	Range of Behavior	Load Factor $K_L$	Mass Factor $K_M$	Load-Mass Factors $K_{LM}$
Simply supported / uniformly distributed load 	Elastic	0.64	0.50	0.78
	Plastic	0.50	0.33	0.66
Simply supported / concentrated load at midspan 	Elastic	1.0	0.49	0.49
	Plastic	1.0	0.33	0.33

Table 2 Descriptions and Corresponding Response Limits of Component (PDC-TR 06-08 2006)

Component Damage Level	Description of Component Damage	Relationship to Response Limits (Table 3)
Blowout	Component is overwhelmed by the blast load causing debris with significant velocities	Response greater than B4.
Hazardous Failure	Component has failed, and debris velocities range from insignificant to very significant	Response between B3 and B4.
Heavy Damage	Component has not failed, but it has significant permanent deflections causing it to be unrepairable	Response between B2 and B3.
Moderate Damage	Component has some permanent deflection. It is generally repairable, if necessary, although replacement may be more economical and aesthetic	Response between B1 and B2.
Superficial Damage	Component has no visible permanent damage	Response is less than B1.

Table 3 Response Limits for Hot Rolled Structural Steel (PDC-TR 06-08 2006)

Member	B1		B2		B3		B4		
	$\mu$	$\theta$	$\mu$	$\theta$	$\mu$	$\theta$	$\mu$	$\theta$	
Flexure	Compact or seismic member		1	3	3°	12	10°	25	20°
	Non compact member		0.7	0.85		1.0		1.2	
	Plate		4	1°	8	2°	20	6°	40
Combined Flexure & Compression	Compact or seismic member		1	3	3°	3	3°	3°	3
	Non compact member		0.7	0.85		0.85		0.85	
Compression		0.9	1.3		2		3		

In design step (A), acceptable maximum component damage levels are defined depending on the level of protection for each building and the component types. The level of protection can be selected by the process described in UFC 4-020-01. According to PDC-TR 06-08 (2006), primary structural components (e.g., column, girder) are required to have a lower component damage level than secondary structural components (e.g., wall, beam) at the same level of protection for the building. Table 2 contains descriptions of component damage for each damage level. With the selected component damage level, a maximum acceptable ductility ratio and a support rotation can be defined by using Table 3, in which  $\mu$  is the maximum allowable ductility ratio and  $\theta$  is the support rotation. For Example, a compact beam is expected to be below Moderate Damage, and the response should be less than B2, as shown in Table 2. Table 3 indicates that response B2, the maximum values of the beam’s ductility ratio and support rotation should be less than 3 and 3°, respectively.

When the charge weight and standoff distance are not defined as design loading, and only the response limits (maximum allowable ductility ratio and support rotation) are given, one of the methods to define the allowable loading for a component with a fixed response limit is to use a Pressure-Impulse (P-I) curve. A P-I curve is a curve representing combinations of pressure and impulse that will cause a predetermined response, in which the pressure-time history is assumed (Krauthammer 2008). Another method is to show charge weight and standoff distance combinations

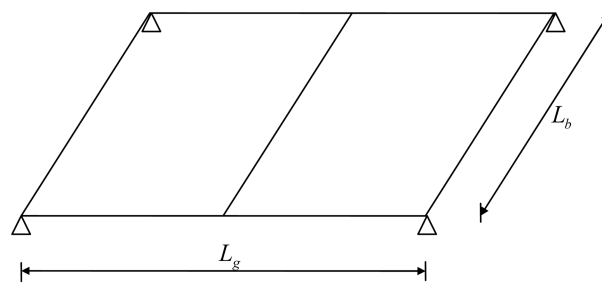


Fig. 1 Roof framing plan

causing a predetermined response limit, which is known as Charge Weight-Standoff Diagrams (CWSD).

Typically, P-I and CWSD curves are derived by using a SDOF model. Although components are connected to each others, typical SDOF analyses are conducted for each component individually by assuming no-interaction between components. Fig. 1 shows a typical roof framing plan, consisting of three beams and two girders with span lengths  $L_b$  and  $L_g$ , respectively.

When the roof is subjected to airblast loading with an uniform pressure time history,  $P(t)$ , SDOF analyses of beams and girders can be conducted separately with following the assumptions in (PDC-TR 06-01 2006):

- A. Simply supported boundaries for both beams and girders
- B. Uniformly distributed load with magnitude of  $P(t)L_g/2$  for beam connected at the midspan of girder
- C. Uniformly distributed load with magnitude of  $P(t)L_g/4$  for beams connected at the ends of girder
- D. Concentrated load  $P(t)L_gL_b/4$  at the midspan for girders

However, since there is a rigid body motion of the beam connected at the midspan of girder due to deflections of the supporting girders, the simply supported boundary assumption can induce errors in the maximum response calculation. The rigid body motion of a beam will also affect the loading applied to girders. Thus, this individual SDOF analysis is expected to be inaccurate for the allowable loadings in both P-I and CWSD curves, due to the neglected rigid body motion of the beams.

In this paper, an inelastic two-degree-of-freedom (TDOF) model was developed to include the beams' rigid body motions for the allowable load calculations, and to examine if the design by the individual SDOF analysis is conservative. The loading is limited to relatively large scaled range cases, where the scaled range (range / charge weight<sup>1/3</sup>) is larger than 1 to ensure a uniformly distributed pressure (Krauthammer 2008).

## 2. Development of two degree of freedom model

A two-degree-of-Freedom (TDOF) model for a roof framing plan (Fig. 1) under uniformly airblast loading,  $P$ , was developed from the force equilibrium equations by assuming negligible damping. Fig. 2 shows force diagrams of beam and girder in the roof framing plan where  $F_g$  represents both the reaction force of a beam, and applied concentrated force to a girder.

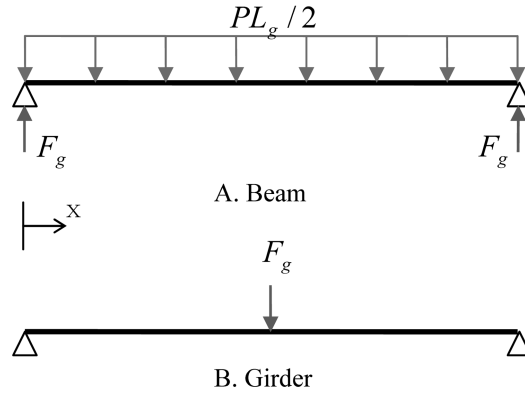


Fig. 2 Force diagrams for beam and girder

From the beam free body diagram in Fig. 2A, the following force equilibrium equation between total applied force and inertia can be derived:

$$F_b - 2F_g = \int_0^{L_b} \rho_b \ddot{d}_b dx = M_b \ddot{u}_g + K_{L_b} M_b \ddot{u}_b \quad (3)$$

where

- $F_b$  :  $(PL_g/2)L_b$ ;
- $P$  : dynamic pressure history applied to roof;
- $F_g$  : reaction force of beam, and applied concentrated force to girder;
- $L_b$  : span length of beam;
- $L_g$  : span length of girder;
- $M_b$  :  $L_b \rho_b$ ;
- $\rho_b$  : mass density of beam;
- $K_{L_b}$  : load factor of beam under uniform loading  
: 0.64 for elastic deformation (Table 1)  
: 0.50 for inelastic deformation (Table 1), and
- $d_b(x, t)$  : displacement of beam  
:  $u_g(t) + u_b(t)Y(x)$ .

where

- $u_g(t)$  : mid-span deflection of girder;
- $u_b(t)$  : mid-span deflection of beam, and
- $Y(x)$  : mode shape function of beam.

Also, since the loading used to deflect the beam is  $F_b - M_b \ddot{u}_g$ , the SDOF force equilibrium equation for beam can be derived

$$K_{LM_b} M_b \ddot{u}_b + R_b = F_b - M_b \ddot{u}_g \quad (4)$$

where,

- $R_b$  : resistance of beam, and

Table 4 Section Properties

Section	Density (kg/m)	Moment of Inertia (mm <sup>4</sup> )	Section Modulus (mm <sup>3</sup> )
A	200	1500000000	5000000
B	200	5000000000	14000000
C	400	5000000000	14000000
D	600	5000000000	14000000

$K_{LM\_b}$  : load-mass factor of beam under uniform loading  
: 0.78 for elastic deformation (Table 1)  
: 0.66 for inelastic deformation (Table 1).

From the force diagram for the girder in Fig. 2B, the following SDOF equation for the girder can be derived

$$K_{LM\_g}M_g\ddot{u}_g + R_g = F_g \quad (5)$$

where

$R_g$  : resistance of girder;  
 $M_g$  :  $L_g\rho_g$ ;  
 $\rho_g$  : mass density of girder, and  
 $K_{LM\_g}$  : load-mass factor of girder under concentrated loading  
: 0.49 for elastic deformation (Table 1)  
: 0.33 for inelastic deformation (Table 1).

By combining the force equilibrium equations [Eqs. (3), (4) and (5)], the inelastic TDOF model equation of the roof can be derived, as follows

$$\begin{bmatrix} 2K_{LM\_g}M_g + M_b & K_{L\_b}M_b \\ M_b & K_{LM\_b}M_b \end{bmatrix} \begin{bmatrix} \ddot{u}_g \\ \ddot{u}_b \end{bmatrix} + \begin{bmatrix} 2R_g \\ R_b \end{bmatrix} = \begin{bmatrix} F_b \\ F_b \end{bmatrix} \quad (6)$$

which can be applied to both linear and nonlinear deformation cases, since resistance functions were used for beam and girder.

### 3. Effect of beam-girder interactions

To show the effects of beam-girder interaction on the allowable loading comparing to the individual SDOF analysis results, P-I and CWSD curves for steel framed roofs (6 m in girder direction, 6 m in beam direction) described in Fig. 1 were generated based on the SDOF model and the proposed TDOF model [Eq. (6)]. Ductility ratios of 1 and 3 were chose as response limits, which are corresponding to the superficial and moderate damage of compact flexural components, respectively (Tables 2 and 3). Three types of roof framing were considered; Type 1 consists of Section B girders and Section A beams, Type 2 consists of Section C girders and Section A beams,

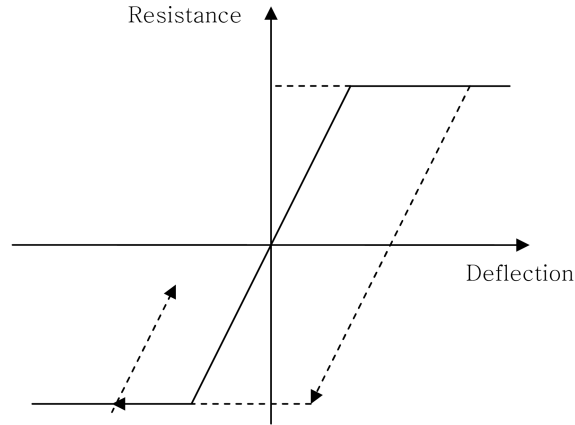


Fig. 3 Resistance function

and Type 3 consists of Section D girders and Section A beams, in which section properties of beams and girders are given in Table 4. The modulus of elasticity and yield stress of steel were assumed as 200 GPa and 345 MPa, respectively.

The resistance functions of beam and girder were assumed to have an elasto-plastic shape, and the slope of the unloading path is the same as the initial stiffness, as shown in Fig. 3. The stiffness in the elastic domain and deflections causing yield are shown in followings (TM 5-1300 1990)

$$K_b = \frac{384EI_b}{5L_b^3} \tag{7}$$

$$K_g = \frac{48EI_g}{L_g^3} \tag{8}$$

$$\text{Max}(R_b) = \frac{8f_y Z_b}{L_b} \tag{9}$$

$$\text{Max}(R_g) = \frac{4f_y Z_g}{L_g} \tag{10}$$

where

- $K_b$  : stiffness of beam in elastic domain of beam resistance function;
- $E$  : modulus of elasticity of steel;
- $I_b$  : moment of inertia of beam;
- $K_g$  : stiffness of girder in elastic domain of beam resistance function;
- $I_g$  : moment of inertia of girder;
- $\text{Max}(R_b)$  : maximum value of beam resistance function;
- $f_y$  : yield stress of steel;
- $Z_b$  : section modulus of beam;
- $\text{Max}(R_g)$  : maximum value of girder resistance function, and
- $Z_g$  : section modulus of girder.

The central difference method (Rao 1995) to solve the SDOF and TDOF model numerically was adopted. The US Army uses the minimum value between 10% of the natural period and 3% of triangular positive loading duration as time step to solve an inelastic SDOF model (PDC-TR 06-01 2006). In this study, the time step was 0.1% of smallest value of natural periods and triangular positive loading duration, which is not efficient in calculating time, but conservative comparing to US Army approach.

For P-I curves, triangular pressure loading histories were assumed, as shown in Fig. 4. It should be noted that the beam failure governs in all TDOF analysis results for Type 1, 2 and 3 roof frames [Some girder failure examples can be found in (Park and Krauthammer 2008)]. Figs. 5-7 show P-I curves from individual SDOF analyses for a beam and a girder, and TDOF analysis for roof frame Type 1, 2 and 3, when the limit ductility ratio was 1. For Type 1 (Fig. 5), if only individual SDOF analysis of beam and girder are used, the designed roof frame is not appropriate for the high peak

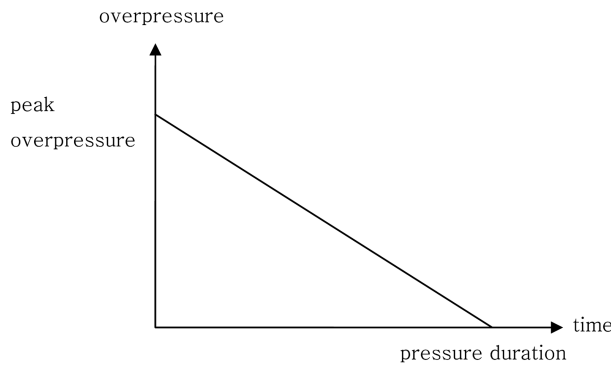


Fig. 4 Right triangular pressure history

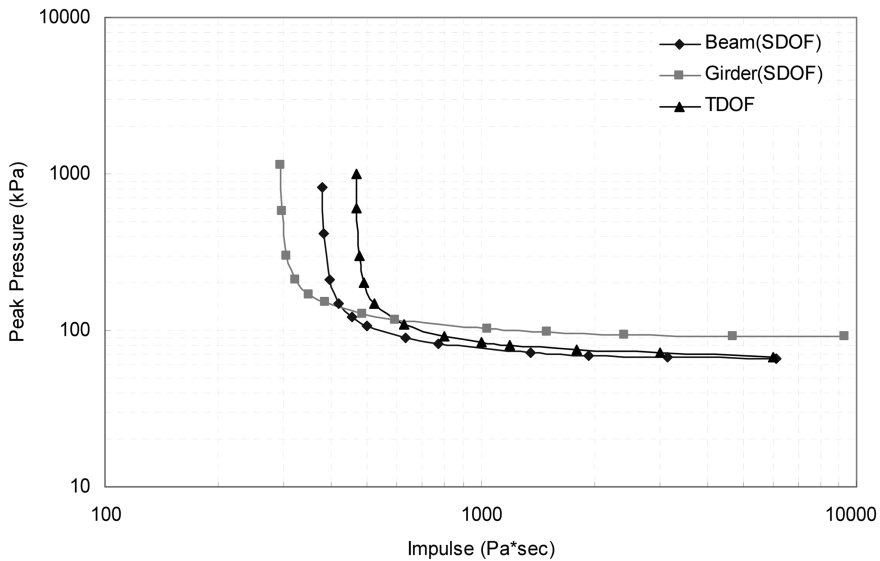


Fig. 5 P-I curves for Type 1 roof from SDOF and TDOF when limit ductility ratio is 1

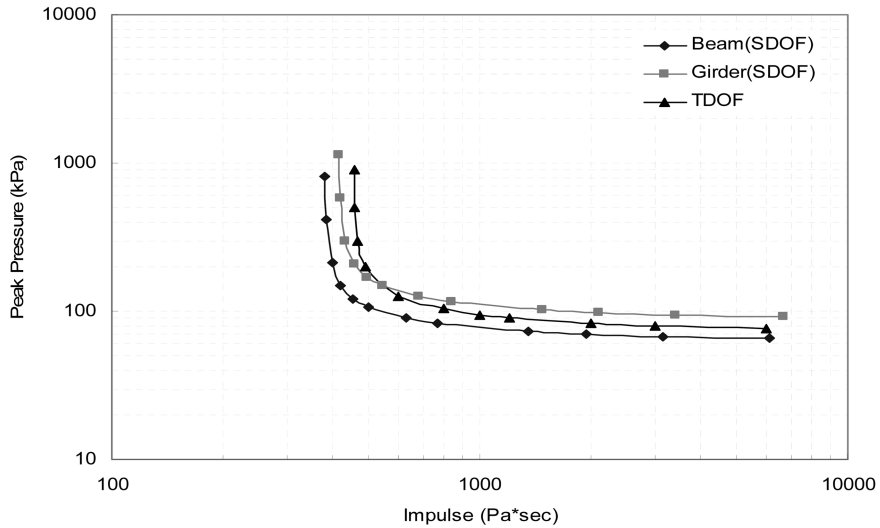


Fig. 6 P-I curves for Type 2 roof from SDOF and TDOF when limit ductility ratio is 1

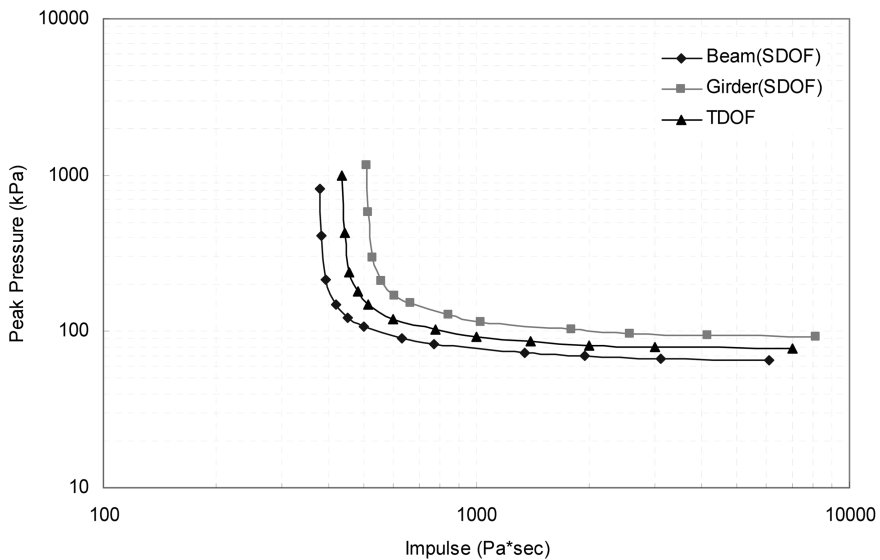


Fig. 7 P-I curves for Type 3 roof from SDOF and TDOF when limit ductility ratio is 1

pressure region, since the girder fails at relatively low loading comparing to the beam in this region. However, since only beam failure was observed in the TDOF analyses of all three roof types, the design of Type 1 can be appropriate for the high peak pressure region. The common observation in Figs. 5-7 is that the individual SDOF analyses lead to conservative loading capacities, as compared to those from the TDOF analysis, due to the rigid body motion of the beam.

CWSD curves were derived by adopting the Kingery and Bulmash equation (Kingery and Bulmash 1984) for the peak over pressure and impulse calculation at a given charge weight and standoff distance. Side-on pressures from hemispherical surface bursts were considered. Fig. 8 shows CWSD curves for the Type 1 roof from SDOF and TDOF simulations, in which limit

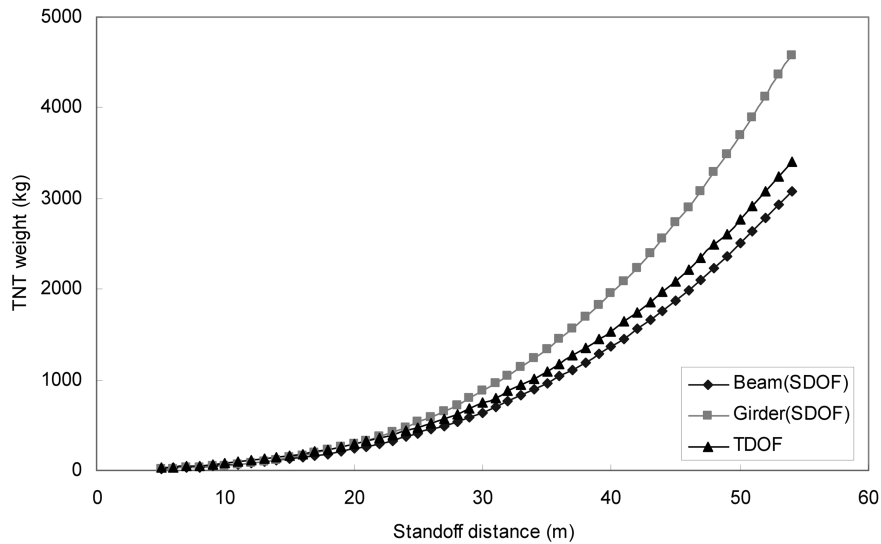


Fig. 8 CWSD curves for Type 1 roof from SDOF and TDOF when limit ductility ratio is 1

Table 5 Allowable TNT weight at given standoff distances for Type 1 roof from SDOF and TDOF analyses when limit ductility ratio is 1

Standoff distance (m)	TNT weight from Beam SDOF analysis (kg) (A)	TNT weight from TDOF analysis (kg) (B)	Difference between results of SDOF and TDOF analyses (%) (B-A)/A
5.00	19.30	25.90	34.20
10.00	59.62	76.88	28.94
15.00	126.28	159.89	26.61
20.00	238.88	289.39	21.14
25.00	406.13	478.90	17.92
30.00	642.18	743.61	15.79
35.00	961.13	1092.51	13.67
40.00	1373.34	1532.16	11.56
45.00	1872.68	2089.25	11.56
50.00	2506.07	2769.51	10.51

ductility ratio is 1. Some of the data in Fig. 8 are presented in Table 5. The individual beam SDOF analysis underestimated allowable TNT charge weight by between 10% and 34%, as comparing those from the TDOF analysis. This shows that the individual beam SDOF analysis is a conservative design tool for this case. For example, if a roof frame was designed to withstand an explosion of 642 kg TNT at a 30 m standoff by adopting the individual beam SDOF model, the roof can actually endure the explosion of 743 kg TNT at 30 m standoff, as shown in Fig. 8 and Table 5. That is, the application of the SDOF model to the Type 1 roof with a limit ductility ratio of 1 results in a 15% underestimation of the load carrying capacity, in terms of the TNT charge weight.

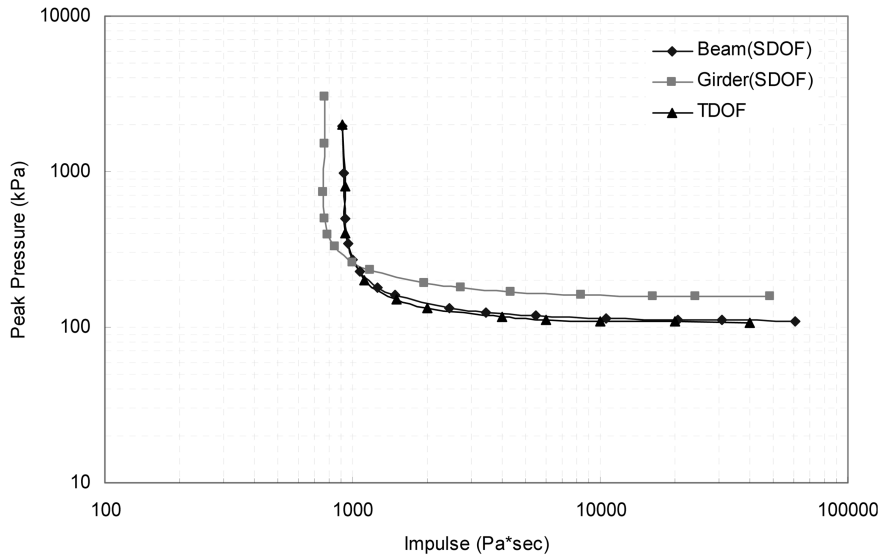


Fig. 9 P-I curves for Type 1 roof from SDOF and TDOF when limit ductility ratio is 3

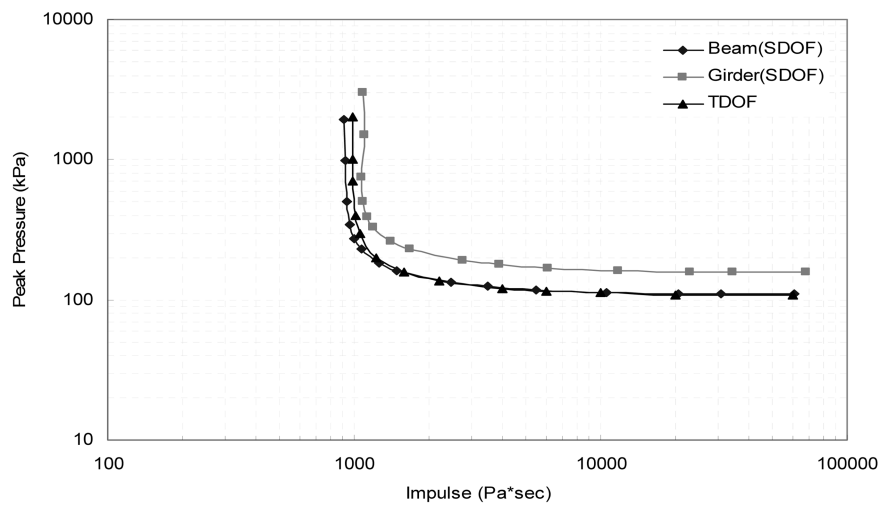


Fig. 10 P-I curves for Type 2 roof from SDOF and TDOF when limit ductility ratio is 3

Figs. 9-11 show P-I curves from individual SDOF analyses for a beam and a girder, and TDOF analysis for roof frame Types 1, 2 and 3, when the limit ductility ratio is 3. Similarly to the previously described case with a limit ductility ratio of 1, the Type 1 frame seems to be reasonably designed, since only a beam failure was observed from the TDOF analyses. It can be clearly observed from Figs. 9-11 that the individual SDOF analyses overestimate the load capacity, as compared to the TDOF analyses. That is, the individual SDOF analysis is not a conservative approach for the case with a limit ductility ratio of 3.

CWSD curves were derived for the Type 1 roof from SDOF and TDOF simulations, in which the limit ductility ratio was 3, as shown in Fig. 12. Some of the data in Fig. 12 are presented in Table 6.

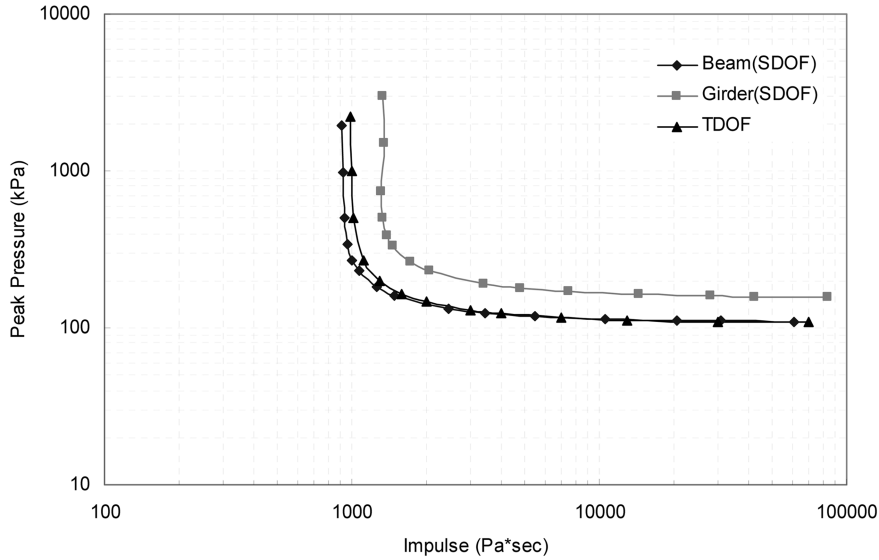


Fig. 11 P-I curves for Type 3 roof from SDOF and TDOF when limit ductility ratio is 3

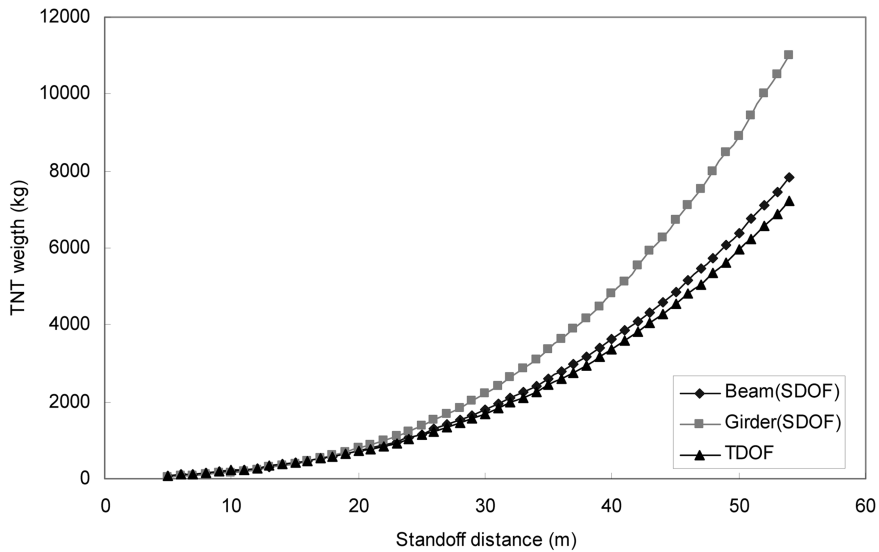


Fig. 12 CWSD curves for Type 1 roof from SDOF and TDOF when limit ductility ratio is 3

Individual beam SDOF analysis underestimated the allowable TNT charge weight by 0.4%, as comparing those from the TDOF analysis when standoff distance was less than around 15 m. However, when the standoff distance was larger than 15 m, individual beam SDOF analysis overestimate the TNT weight by maximum of 7% (Table 6). Thus it can be said that the individual beam SDOF analysis is an unconservative design tool for this case. For example, when 6371 kg TNT explode at a 50 m standoff distance, a roof frame designed by the individual beam SDOF model can not withstand the design load since the roof frame can endure only the explosion of 5949 kg of TNT, as simulated by the TDOF. To explain why the individual SDOF analysis

Table 6 Allowable TNT weight at given standoff distances for Type 1 roof from SDOF and TDOF analyses when limit ductility ratio is 3

Standoff distance (m)	TNT weight from Beam SDOF analysis (kg) (A)	TNT weight from TDOF analysis (kg) (B)	Difference between results of SDOF and TDOF analyses (%) (B-A)/A
5.00	76.50	76.80	0.39
10.00	209.80	210.62	0.39
15.00	418.15	416.14	-0.48
20.00	730.28	707.48	-3.12
25.00	1165.43	1139.30	-2.24
30.00	1792.27	1689.51	-5.73
35.00	2609.05	2436.68	-6.61
40.00	3625.13	3353.99	-7.48
45.00	4851.24	4530.74	-6.61
50.00	6370.14	5949.30	-6.61

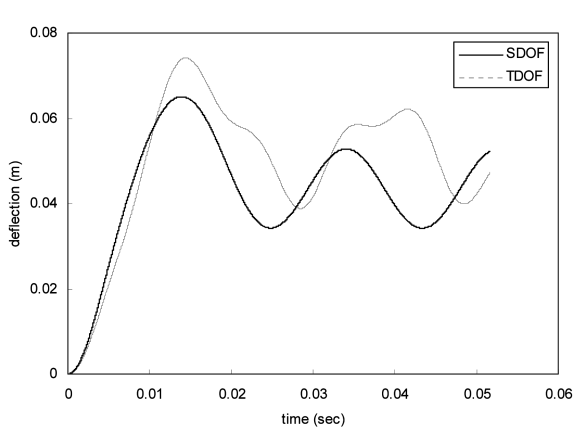


Fig. 13 Time history of beam deflections from SDOF and TDOF

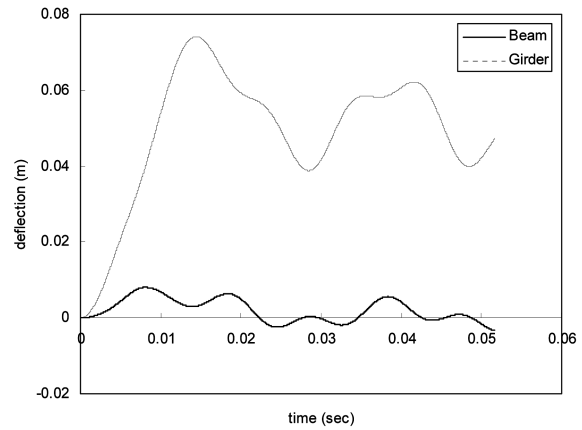


Fig. 14 Time history of beam and girder deflections from TDOF

overestimates load carrying capacity in this case, the time histories of beam deflections were simulated by using SDOF and TDOF analyses with a fixed loading conditions (standoff distance = 50 m, TNT weight = 6371 kg), as shown in Fig. 13. The individual SDOF analysis clearly underestimates the maximum deflection comparing to that from the TDOF model. At the early time (within 0.008 sec), the SDOF model overestimated the deflection due to the rigid body motion of the girder moving in the direction of loading. However, as shown in Fig. 14 where deflections of the girder and beam were simulated with the TDOF analysis, the girder deflected in opposite direction of loading after 0.008 sec. This means that negative acceleration of the girder occurred at some time before 0.008. This will increase the flexural loading in the right side of Eq. (4). Thus, it may be concluded that using an SDOF analysis could be a conservative design approach if the time corresponding to the maximum beam deflection is less than the time inducing the negative girder acceleration.

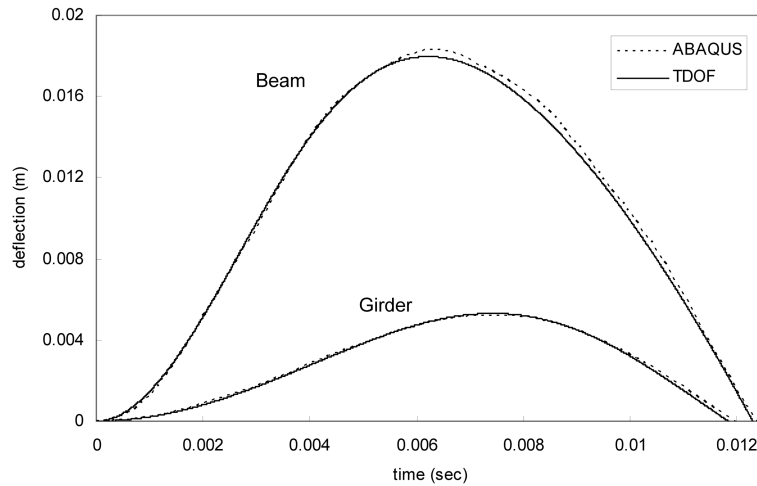


Fig. 15 Deflection histories from ABAQUS and TDOF models

Deflection histories of a Type 1 roof frame under triangular pressure (Fig. 4) with a maximum pressure 200 kPa and duration of 4 ms were estimated by using the TDOF and finite element model to check the validity of the proposed TDOF model. The finite element model was prepared using ABAQUS/Explicit with Timoshenko beam elements B31 (ABAQUS 2006). Fig. 15 shows the deflection histories of the beam and girder from the TDOF and ABAQUS models. The differences between the maximum girder and beam deflections for the two models are 2.05% and 1.77%, respectively. Thus, it can be concluded that the proposed TDOF model is a reasonably accurate analysis tool.

#### 4. Conclusions

An inelastic two-degree-of-freedom model was developed to account for the rigid body motion of beams in a roof frame. It was shown with P-I and CWSD curves that ignoring this rigid body motion results in both underestimating and also overestimating the load carrying capacity. This overestimation can be significant since the SDOF analysis has been considered as a conservative approach. Thus, further research is recommended to determine the limitation of the SDOF application by obtaining closed form or approximated solutions of P-I curves from the proposed TDOF model. Although the presented P-I and CWSD curves are based on first bending modes, the proposed model can be also used for other responding mode shapes if corresponding resistance function, load and load-mass factors are given.

#### References

- ABAQUS (2006), "ABAQUS 6.6 Documentation: Analysis User's Manual, Theory Manual".  
 Army TM 5-1300 (1990), "Structures to resist the effects of accidental explosions", US Department of the Army.  
 Army TM 5-855-1 (1986), "Fundamentals of protective design for conventional weapons", US Department of

- the Army.
- Kingery, C.N. and Bulmash, G. (1984), "Technical report to ARBRL-TR-02555: Airblast parameters from TNT spherical air burst and hemispherical surface burst", US Army Ballistic Research Laboratory.
- Krauthammer, T. (2008), *Modern Protective Structures*, CRC Press.
- Park, J.Y. and Krauthammer, T. (2008), "Beam-girder interactions for roof damage analysis under explosive loading", *The Proceedings of 4<sup>th</sup> International Conference on ASEM08*, Korea.
- PDC-TR 06-01 (2006), "Methodology manual for the single-degree-of-freedom blast effects design spreadsheets", US Army Corps of Engineers.
- PDC-TR 06-08 (2006), "Single degree of freedom structural response limits for antiterrorism design", US Army Corps of Engineers.
- Rao, S.S. (1995), *Mechanical Vibrations*, Addison-Wesley.
- UFC 4-020-01 (Pending), "DoD security engineering facilities planning manual", US Department of Defense.